Volume 18 | Number 18 | 21 September 2018 | Pages 2677–2884

Lab on a Chip

Devices and applications at the micro- and nanoscale

rsc.li/loc

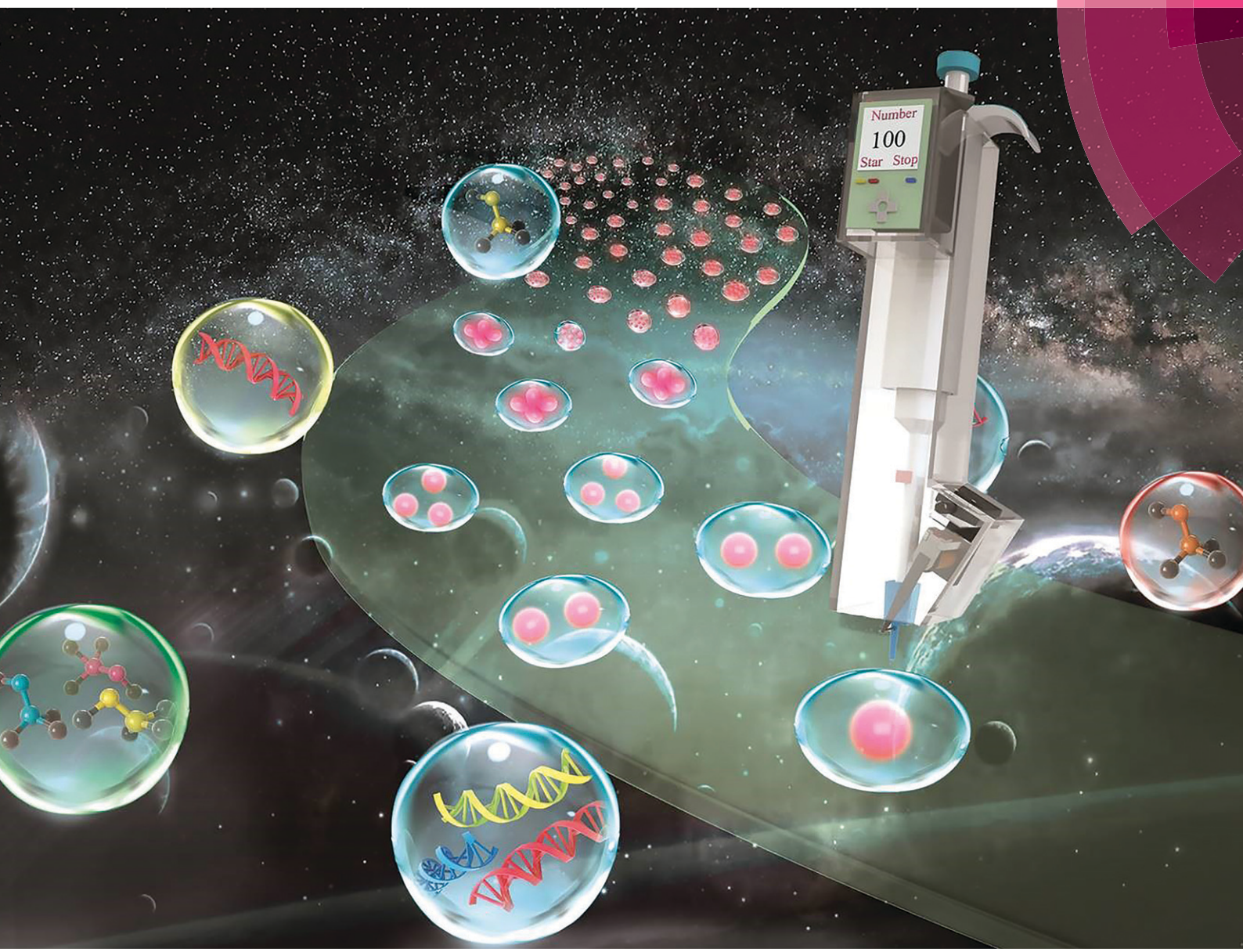

ISSN 1473-0197

ROYAL SOCIETY OF CHEMISTRY

PAPER

Baoqing Li, Tingrui Pan *et al.*

High-precision digital droplet pipetting enabled by a plug-and-play microfluidic pipetting chip

Published on 10 July 2018. Downloaded by University of Science and Technology of China on 4/15/2019 4:57:58 AM.

Lab on a Chip

PAPER

View Article Online
View Journal | View Issue

Check for updates

Cite this: *Lab Chip*, 2018, **18**, 2720

High-precision digital droplet pipetting enabled by a plug-and-play microfluidic pipetting chip†

Yuxin Mao, [a] Yang Pan,[a] Xuan Li, [a] Baoqing Li, *[a] Jiaru Chu[a] and Tingrui Pan *[bc]

Received 17th May 2018,
Accepted 6th July 2018

DOI: 10.1039/c8lc00505b

rsc.li/loc

Emerging demands for handling minute liquid samples and reagents have been constantly growing in a wide variety of medical and biological areas. This calls for low-volume and high-precision liquid handling solutions with ease-of-use and portability. In this article, a new digital droplet pipetting method is introduced for the first time, derived from the microfluidic impact printing principle. Configured as a conventional handheld pipette, the prototype device consists of a plug-and-play and disposable microfluidic pipetting chip, driven by a programmable electromagnetic actuator for on-demand dispensing of nanoliter droplets. In particular, the impact-driven microfluidic pipetting chip, in place of the traditional disposable pipette tips, offers both liquid loading and droplet generation. The printing nozzle has been microfabricated using a femtosecond laser with a super-hydrophobic structure, in order to minimize the dispensing residues. As a result of the high-precision droplet dispensing principle, the variations of the dispensed volume have been successfully reduced from 49.5% to 0.6% at 0.1 μL, as compared to its commercial counterparts. A proof-of-concept study for concentration dilution and quantitative analysis of cell drug resistance has been carried out by using the digital droplet pipetting system, demonstrating its potential in a broad range of biomedical applications which require both high precision and low-volume processing.

Introduction

Liquid handling, by means of metering, blending, and separating samples and reagents, has been involved in almost every aspect of contemporary biomedical and clinical applications, ranging from fundamental research to medical diagnoses.[1–3] The trend driving towards further facilitation and miniaturization of biomedical analyses provides appealing opportunities with potential technological advantages including high-throughput low reagent consumption and high detection sensitivity.[4–10] Recently, microplate pipetting has taken center stage for biochemical analyses,[11–13] as it is intended to address the aforementioned challenges. As the industrial efforts continuously evolve, the robotic components and automation solutions have been extended to the liquid-handling device family. These automated dispensing instruments have been widely deployed in industrial-scale screening and production work due to their high robustness and high reliability with increased throughput in automated liquid processing,[14–17] while the conventional handheld micropipettes continue to serve as the gold standard for volumetric quantitative liquid handling in laboratory and R&D settings, because of their reliability, portability and convenient-to-use features.

Established on the piston-driven air displacement mechanism, micropipettes can be used to effectively handle liquid samples between 1 μL and 1000 μL.[18–21] Handling a smaller volume (below 1 μL), based on the same principle, faces insurmountable technical hurdles, such as compressibility of the air volume, inevitable liquid contact, and consequential adherence onto the pipette tip. As a result, the deviations from the targeted volume can be as significant as more than 20% in such a range.[4,20–24] This level of error can potentially lead to detrimental results in subsequent quantitative determinations.[25] It poses a volumetric limitation on further miniaturization for biochemical analyses, and therefore, the current standard to avoid this level of inaccuracy is to have the analysis conducted at the smallest volume transfer greater than 1 μL, which could lead to unnecessary expense of costly reagents and labor.[25,26]

The latest efforts on integrating the traditional micropipettes with the microfluidic principles have extended their application to new capacities. For example, the Coltro group

[a] *Department of Precision Machinery & Precision Instrumentation, University of Science & Technology of China, Hefei, Anhui, 230027, China. E-mail: bqli@ustc.edu.cn*
[b] *Department of Biomedical Engineering, University of California, Davis, 95616, USA. E-mail: trpan@ucdavis.edu*
[c] *Shenzhen Institutes of Advanced Technology, Chinese Academy of Sciences, Shenzhen, Guangdong, 518055, China*

† Electronic supplementary information (ESI) available. See DOI: 10.1039/c8lc00505b

This journal is © The Royal Society of Chemistry 2018

Published on 10 July 2018. Downloaded by University of Science and Technology of China on 4/15/2019 4:57:58 AM.

combined an electronic micropipette with a microfluidic chip to perform electrophoresis analysis.[27] The Beebe group has presented a passive microfluidic method by using a single pipette for cell-based assays.[28] The Garstecki group incorporated micropipettes into a microfluidic chip as a step emulsificator and generated libraries of nanoliter-size droplets.[29] Additionally, the Qin group reported that incorporating a custom micropipette tip with embedded microchannels into a conventional micropipette allowed easy and fast isolation of individual cells in nanoliter volumes for single-cell sequencing.[30,31] Although the above-mentioned improvements involved microfluidic innovations and showed new functionalities, they didn't directly address the essential technical limitation of micropipetting, *i.e.*, inaccuracies in low-volume liquid processing.

Meanwhile, microfluidic-generated nanoliter and picoliter droplets have been increasingly utilized as miniature compartmentalized reaction chambers, which is a highly active direction of research in fields, such as immunology, pharmacology, and synthetic and molecular biology,[6,32–34] benefiting from their small and highly uniform volumes. Among those efforts, drop-on-demand droplet dispensing through a printing nozzle, similar to commercial inkjet printing, has shown great promise in generation of quantitative liquid volumes from the picoliter to nanoliter range.[35–42] Several pieces of droplet dispensing equipment have been recently made commercially available as the latest generation of automated liquid handling tools, including Biojet Elite™, Tecan D300e™ and BioFluidix PipeJet™ dispensers, all claiming to have high reliability and accuracy for low-volume operations (in nanoliter ranges). However, the high equipment cost, bulky footprint, and initial volume requirements along with complicated user interfaces have restricted their applications for portable, highly customary and exploratory experimentation in a research setting.[4] Thus, it is still high desirable for laboratory researchers to have an easy-to-use, high-accuracy, portable device in low-volume liquid processing settings, where both high precision and high flexibility are demanded.[1,22,42] Recently, the microfluidic impact printing (MIP) approach has been introduced by the Pan group.[35–37] The MIP system utilizes a modular microfluidic cartridge design to generate consistent nanoliter droplets in a non-contact mode. It is comprised of an interchangeable microfluidic cartridge with printing nozzles and separable external actuators, allowing precise dispensing of multiple fluidic contents, from which the target volume is calculated by multiplying the unit volume of ejected droplets and the number of ejections from the device.

In this paper, we introduce for the first time a novel high-precision digital droplet pipetting method, derived from the original MIP principle mentioned above,[35–37] in which consistent droplets can be ejected out from the microfluidic cartridge in a non-contact mode. Configured as a conventional handheld pipette, the prototype device consists of a plug-and-play and disposable microfluidic cartridge with a high-precision loading and dispensing nozzle, driven by a programmable electromagnetic actuator for on-demand dispensing of nanoliter droplets. In particular, the impact-driven microfluidic pipetting chip with a built-in nozzle, in place of the traditional disposable pipette tips, offers both liquid loading and droplet generation. The printing nozzle has been precisely microfabricated using a femtosecond laser with a superhydrophobic structure, in order to minimize liquid residues from aspirating and dispensing. Due to the highly consistent droplet dispensing method based on microfluidic impact printing, the targeted volume ranges from nanoliters to microliters with a nanoliter resolution can be achieved by multiplying the number of ejections. As a result, the variations of the dispensed volume have been successfully reduced from 49.5% to 0.6% at 0.1 μL, as compared to its commercial counterparts. Using the digital droplet pipetting prototype, experimental studies for quantitative analysis of concentration dilution and cell drug resistance have been conducted successfully, demonstrating its potential in a broad range of biomedical applications, where both high precision and low-volume processing are required.

Working principle

As illustrated in Fig. 1a–c, the digital droplet pipetting device, configured on the external body of a manual micropipette, includes an exterior plastic case amounted onto the pipette, a control unit with programmable electronics and a user interface, connected with an electromagnetic actuator which drives a plug-and-play microfluidic pipetting chip with a built-in loading and dispensing nozzle, to replace the conventional pipette tips. In addition, a pneumatic valve has been implemented to modify the air path of the pipette body, from which the loading and dispensing phases can be determined. As the core component, the microfluidic pipetting chip offers combined functions of liquid loading, storage, and droplet dispensing. In particular, the reversible design of the pluggable microfluidic pipetting chip with the in-plane tapered nozzle, similar to a traditional disposable pipette tip (in Fig. 1d), allows aspirating the liquid and dispensing droplets from the same path as well as easy alignment with the targeted position. Moreover, the nozzle tip has been precisely laser-micromachined and superhydrophobically-treated using a femtosecond pulsed laser system to ensure both consistent generation of nanoliter droplets during dispensing and minimal liquid adherence after aspiration. When the valve closes, the microfluidic pipetting chip is pneumatically connected to the air-displacement mechanism of the manual pipette, from which liquid aspiration can take place, similar to that of a regular pipette tip (in Fig. 1e). Once the pneumatic valve switches open, the device enters into the dispensing mode, in which droplet ejection can be triggered by the adjacent electromagnetic actuator, based on our microfluidic impact printing principle.[35–37] Specifically, the deformable membrane displaces the liquid inside the microfluidic cartridge once the actuator strikes the membrane. According to the resistance design of the microfluidic channels, a portion of the

Published on 10 July 2018. Downloaded by University of Science and Technology of China on 4/15/2019 4:57:58 AM.

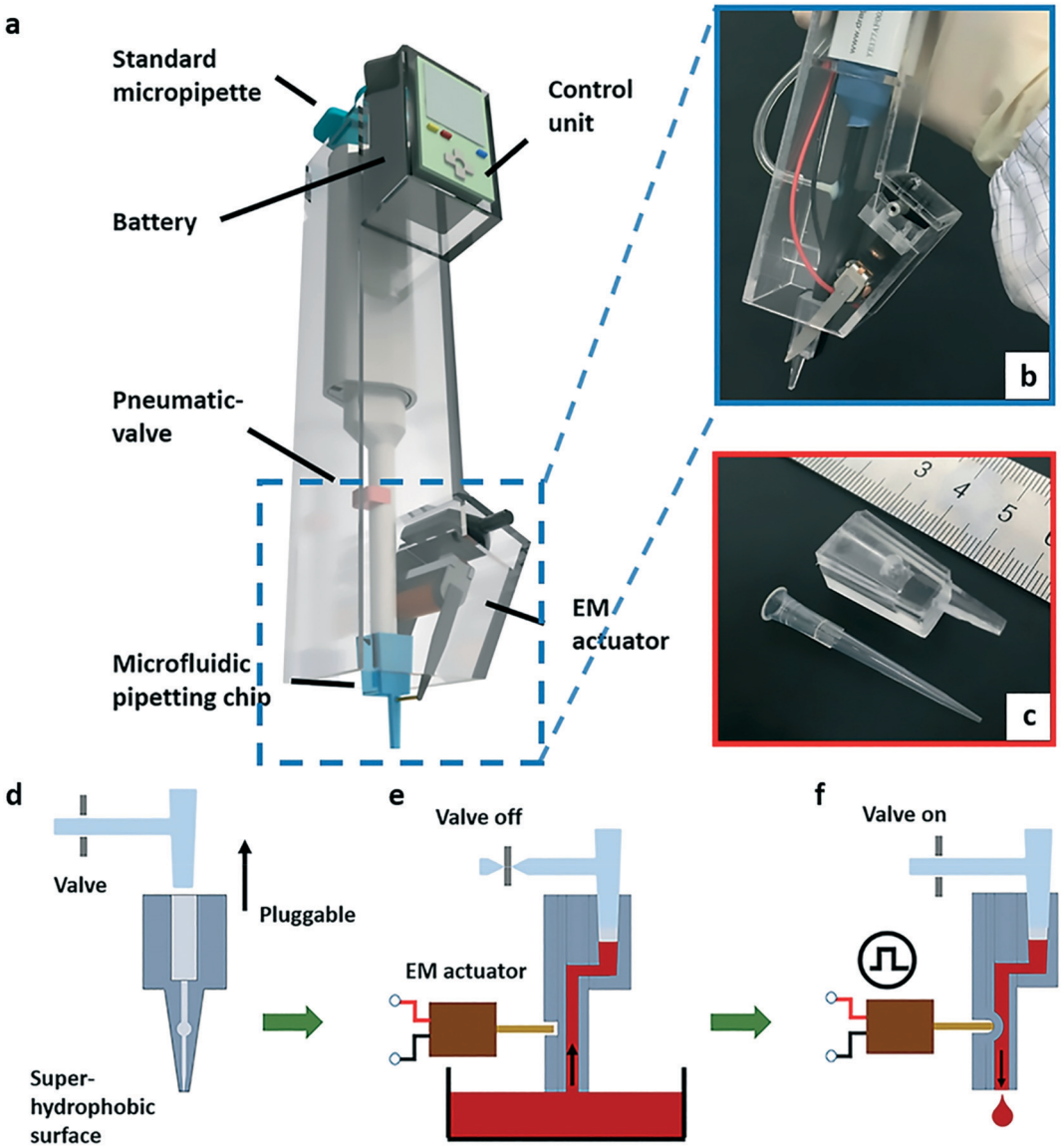

Fig. 1 a) Systematic diagram of the digital droplet pipetting system, composed of a reversibly pluggable microfluidic pipetting unit and attached onto a conventional micropipette. b) Photographs of the microfluidic pipetting chip mounted on the exterior case, and c) a comparison between the microfluidic pipetting chip and a standard micropipette tip (of 0.1–10 μL). Operation procedures of the digital droplet pipetting: d) first, mount the microfluidic pipetting chip onto the micropipette; e) switch off the pneumatic valve to connect to the air-displacement mechanism of the manual pipette, from which liquid aspiration can take place, similar to that of a regular pipette tip (aspiration mode); f) once the pneumatic valve switches open, the device enters into the dispensing mode, in which droplet dispensing can be triggered by the adjacent electromagnetic actuator (dispensing mode).

displacement volume towards the nozzle would cause droplet ejection, as shown in Fig. 1f. Benefiting from the highly consistent droplet dispensing mechanism, the targeted volume ranges from 5 nL to 10 μL with a tunable single-droplet resolution between 5 nL and 10 nL, which can be achieved by multiplying the number of ejections.

Methods and materials

Design and fabrication of the microfluidic pipetting chip

The microfluidic pipetting chip was designed to contain four functional layers, a strengthening layer, a deformable membrane layer, a microchannel layer, and a reversibly pluggable reservoir (from bottom to top, Fig. 2a). The microchannel was laid out by using AutoCAD software (Autodesk) and fabricated by photolithography and polydimethylsiloxane (PDMS) replica molding techniques. Specifically, utilizing photolithography, a 75 μm thick microchannel structure of negative photoresist (MicroChem SU-8 2025) was photo-patterned on a glass. Successively, polydimethylsiloxane prepolymer at a 10 : 1 ratio (Dow Corning SYLGARD184) was mixed and degassed under vacuum for 15 min, followed by pouring it onto the photoresist mold with 2 mm thickness and curing at 65 °C for 2 hours. After curing, the

 This journal is © The Royal Society of Chemistry 2018

Published on 10 July 2018. Downloaded by University of Science and Technology of China on 4/15/2019 4:57:58 AM.

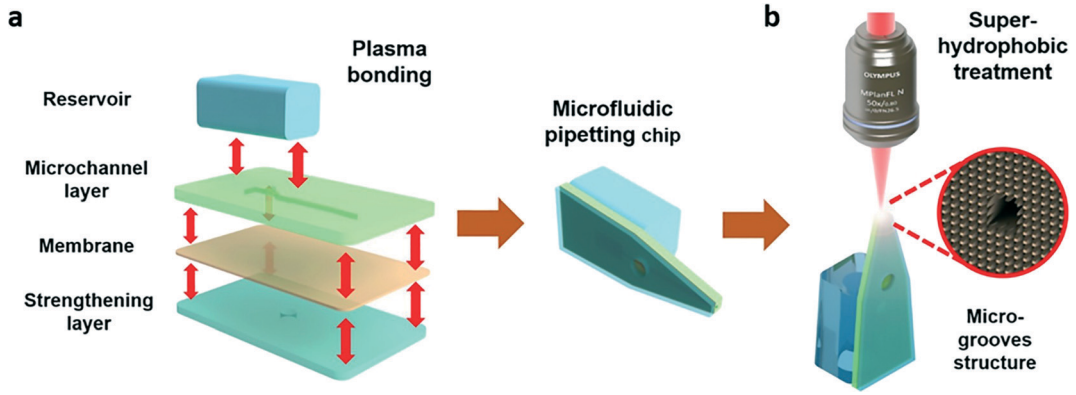

Fig. 2 a) Illustrations of the microfluidic pipetting chip fabricated by plasma bonding with four functional layers, *i.e.*, a strengthening layer, a deformable membrane layer, a microchannel layer, and a reversibly pluggable reservoir (from bottom to top). b) Super-hydrophobic surface treatment on the dispensing nozzle using a femtosecond laser machine.

microchannel-patterned PDMS layer was detached and a through-hole was punched to connect to the top reservoir. Another 250 μm-thick planar PDMS film was prepared as the deformable membrane. The mechanical strengthening layer is a 1.5 mm-thick PDMS substrate, intended to reinforce the device structure and to prevent channel collapse. For the reversibly pluggable reservoir, an aluminum master mold was fabricated using a CNC milling machine. At the assembly step, all four PDMS layers were treated with oxygen plasma (Mingheng PDC-MG, 50 s, 75 W, 100 Pa). With an alignment protocol, the chip was treated at 65 °C for 30 min to complete bonding. Next, the dispensing nozzle was manually trimmed under a microscope using a scalpel. Finally, the micro-nozzle surface was treated to possess super-hydrophobicity using a regenerative amplified Ti:sapphire femtosecond laser system (Coherent, Chameleon Vision-S/Legend Elite F HE-1K) (Fig. 2b).

Calibration methods

During the calibration, deionized water was used as the calibration agent. Two methods were used to evaluate the precision of the digital liquid-handling device. One was to use high-speed photography, followed by image analysis. In such a measurement, 300 to 400 droplets were generated by the dispenser and monitored using a stroboscope (Photron FASTCAM SA5) with 7× magnification. The images were analyzed in a MATLAB scrip to compute the diameters and the coefficients of variation (CV) for these droplets.[43,44] A gravimetric characterization method using a microbalance (Sartorius CPA225D, 0.01 mg resolution) was implemented to calibrate the droplet weight/volume.[43,44] In consideration of the measurement adequacy, the total mass of the dispensed droplets was set in the range between 0.5 mg and 5.5 mg by continuous droplet generation (100 to 500 droplets). In order to minimize the evaporative effects of deionized water during the measurement, droplets were printed into a Petri dish, which was covered by a 3 mm-thick layer of mineral oil (Sigma-Aldrich M8410).

Concentration dilution methods and measurements

Fluorescence characterization experiments were conducted on concentration gradients generated by two pipetting methods, one is the digital droplet pipetting method, in which the targeted concentrations have been achieved by directly adding sample and buffer solutions together in one step, as compared to the two-step dilution procedure operated by using a commercial micropipette (Finnpipette™F1 with 0.2–2 μL and 20–200 μL pipette tips).[45] Sodium fluorescein ($C_{20}H_{10}Na_2O_5$) with a high concentration (10 mg mL^{-1}) was used as a model sample and deionized water as a solvent to create a series of low concentration gradients (0 μg mL^{-1} to 10 μg mL^{-1}) in a 96-well plate with 6 replicates.[15] By using the digital droplet pipette, different volumes (0.01–0.1 μL) of sodium fluorescein samples were directly added into deionized water to achieve a series of concentrations. When using the standard micropipette, 20 μL sample was firstly added to 380 μL deionized water. Next, the diluted samples (0.2–2.0 μL) were further diluted in deionized water to generate the desired concentrations. The total volume of solution in each well is 100 μL. The intensity of the fluorescence was measured using a fluorescence microscope (Leica DMI3000b).

Drug resistance analysis

A549 cell lines (Cell Bank of Chinese Academy of Sciences) were cultured in Dulbecco's Modified Eagle Medium (DMEM) supplemented with 10% fetal bovine serum and 1% streptomycin/penicillin (Gibco culture medium) and incubated at 5% CO_2, 37 °C. After the cells reached confluency, they were trypsinized, centrifuged and resuspended in fresh culture medium. The cells were subsequently seeded on substrates and incubated at 8×10^3 cells with 100 μL culture medium per well in 96-well microplates. Then, cell plating treatment was carried out using different doxorubicin concentrations for 24 h. In the procedure of the experiment, doxorubicin (5 mg mL^{-1}, 0.01–1 μL) was added into 100 μL culture medium containing A549 cells by using the digital droplet pipette, and a series of concentrations of doxorubicin (0.1–10 μM) were

Published on 10 July 2018. Downloaded by University of Science and Technology of China on 4/15/2019 4:57:58 AM.

achieved. The control experiment was carried out using a micropipette; the concentration of doxorubicin was firstly diluted to 0.1 mg mL^{-1}. Then, different volumes of doxorubicin (0.3–6 μL) were added into the wells containing 100 μL of culture medium and A549 cells; the final concentrations of doxorubicin were from 0.5 μM to 10 μM. Cell viability was assessed using the CCK-8 assay in a microplate reader. 10 μL of CCK-8 was added to each well, and the microplate was incubated at 37 °C for 2 hours in a 5% CO_2 humidified incubator. The absorbance was then measured at 450 nm by using a microplate spectrophotometer (Molecular Devices SPECTRAmax®190). Cell viability was expressed as a percentage of the control cell culture value. A control experiment was performed in parallel to monitor the influence of DMEM on the assays. The cell viability was calculated as follows: cell viability = $100\% \times (OD_{test} - OD_{blank})/(OD_{control} - OD_{blank})$.

Results and discussion

Design and fabrication of the microfluidic pipetting chip

The microfluidic pipetting chip has a comparable size (30 mm long) to that of a conventional tip (40 mm long of 0.1–10 μL), and similarly, it is also easy-to-mount, disposable and suitable for one-handed operation, as shown in Fig. 1c. The nozzle sizes here are set at 95 μm, 126 μm, and 270 μm, respectively, at a height of 75 μm. These are determined by the dimensions created in the SU8 mold and can be adjusted by the lithography process. An ultra-low dead volume could reduce reagent consumption and save cost, especially for expensive biological reagents.

Superhydrophobicity of the printing nozzle

One challenge in microfluidic droplet printing is that the liquid contents tend to adhere onto the tip surface during aspiration, which can potentially block the nozzle and prevent subsequent droplet dispensing. To address this issue, a superhydrophobic treatment on the dispensing nozzle has been conducted. Recently, nanostructured surfaces have been frequently adopted to establish high-performance superhydrophobic surfaces, offering exceptional non-adherence properties from the liquid.[46–48] We have applied a femtosecond-pulsed-laser direct writing system to perform the surface treatment on the PDMS nozzle surface. The superfast pulsed laser system has ultrahigh instantaneous laser power to etch high-definition patterns, while protecting the surface from potential thermal ablation by low average-power, which makes it ideal for fabricating combined micro- and nanostructures on different substrates.[49–52] Upon its contact with the liquid substance, the irradiated PDMS surface traps tiny air bubbles among its micro- and nanotopology, making it resistant to liquid adherence and superhydrophobic. Markedly, though it offers a permanent physical modification of the PDMS surface with superhydrophobicity, the superfast pulsed laser machining keeps the original biocompatibility of PDMS without adding extra chemicals.[52]

We have further investigated the relationship between the surface superhydrophobicity and the laser treatment parameters (both the power setting and scanning mode). Fig. 3 illustrates the change of water CAs under different laser power settings (*i.e.*, 30 mW, 90 mW and 150 mW) and grid periods (*i.e.*, scanning patterns), together with the corresponding SEM images of their surface topologies. As can be seen, the laser power has a direct influence on the fabricated microstructures, for instance, the measured depths of the engraved micropatterns are 11 μm, 24 μm and 18 μm, respectively. As a result, at a lower power setting of 30 mW, the CA is measured to be less than 115°, exhibiting a marginal improvement on the hydrophobicity. This is possibly due to an insufficient height of the laser-etched microgrooves (in Fig. 3c). At an elevated power mode of 90 mW, a superhydrophobic effect (CA > 150°) has started to emerge with a grid period in the range of 10 μm to 120 μm (in Fig. 3d). With a further increase in the laser power (to 150 mW), the CA has shown a trend of slight decrease compared to that at 90 mW, which may also be factored by the reduced structure depth due to thermal ablation effects in the unpatterned areas (in Fig. 3e). On the other hand, the period of the laser grid, as one measure of the scanning mode, has also shown a substantial effect on the surface superhydrophobicity. For example, as the period rises from 120 μm to 400 μm at a power level of 90 mW, the surface superhydrophobicity decreases possibly resulting from an increased contact area between water and the untreated surface. Likewise, similar results appear with large grid periods at a power setting of 150 mW, however, for a grid size less than 90 μm, when the water CA is elevated due to decreased surface ablation at the increased period, which reaches the peak point at the period of 90 μm. Furthermore, differences in the surface topologies between the laser irradiated and unprocessed nozzle surfaces have been investigated. For instance, Fig. 3f and g illustrate the scanning microscopic images of the superhydrophobically treated surface with a control, which has been processed at a laser power of 90 mW and a scanning period of 30 μm. In brief, the laser-etched micro- and nanostructures established by different laser machining settings can be crucial in determining the surface superhydrophobicity of the non-adherence dispensing nozzle.

As aforementioned, the surface hydrophobicity could have a considerable impact on the performance of droplet dispensing. As can be seen from the microscopic views, no appreciable liquid content surrounding the nozzle has been observed with the superhydrophobically treated nozzle (in Fig. 3h). Meanwhile, without a surface superhydrophobic treatment, fluid accumulation could occur immediately following liquid contact or aspiration (in Fig. 3i). More importantly, the surface superhydrophobic treatment noticeably extends the printing performance of the nozzle. As shown in the microscopic photos, the superhydrophobically-treated microfluidic nozzle hasn't formed any appreciable liquid accumulation after 1000 prints (in Fig. 3j). In contrast, the control nozzle shows evident liquid adherence from satellite droplets after the same number of printing (in Fig. 3k).

 This journal is © The Royal Society of Chemistry 2018

Published on 10 July 2018. Downloaded by University of Science and Technology of China on 4/15/2019 4:57:58 AM.

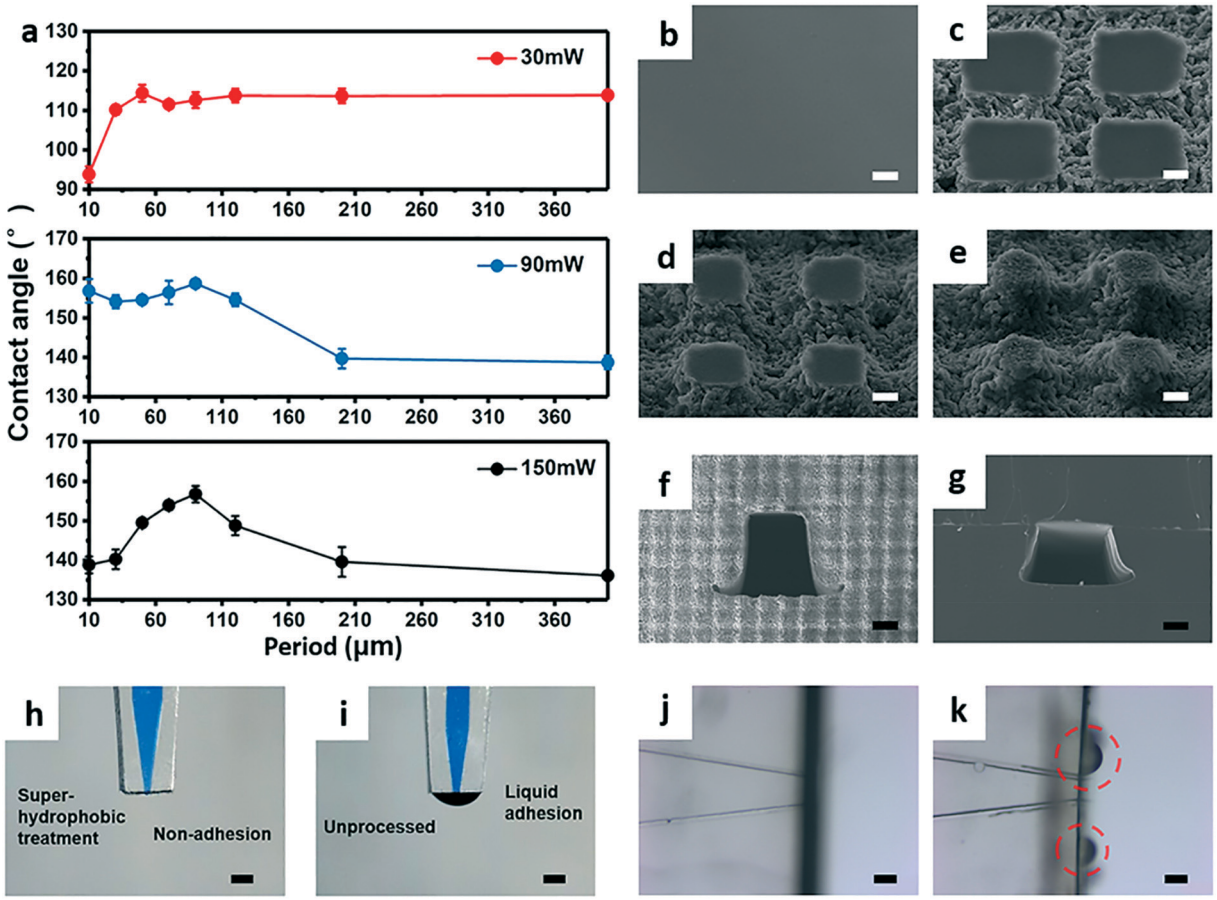

Fig. 3 a) Relationships between the grid periods and the water CAs under different laser power settings (30 mW, 90 mW and 150 mW). SEM picture of b) unprocessed and c)–e) super-hydrophobic PDMS surfaces with 50 μm period of grid microgrooves. The PDMS surfaces were processed at laser powers of c) 30 mW, d) 90 mW and e) 150 mW (scale bar: 20 μm). f) SEM picture of super-hydrophobic (30 μm period, 90 mW laser power) and g) unprocessed nozzle surfaces (scale bar: 40 μm). h) and i) Two microfluidic pipetting chips with different nozzle surfaces immersed in deionized water containing blue dye; fluid accumulation occurred at the unprocessed nozzle surface (scale bar: 200 μm). j) and k) The picture of the chip nozzle after printing 1000 droplets; liquid adheres to the chip's tip around the nozzle (in the red circles) without super-hydrophobic treatment (scale bar: 25 μm).

Characterization of droplet dispensing

As described in Methods and materials, the performance of droplet printing has been evaluated by both high-speed high definition image analysis and gravimetric characterization. Fig. S1† shows the schematic illustration of the droplet size calibration using high-speed photography. The high-speed sequential images of a typical droplet dispensing process are illustrated in Fig. 4a. As can be seen, upon the compression of the liquid content, driven by the impactful EM actuation towards the microfluidic pipetting chip, it is accelerated towards the nozzle, and once the fluidic inertia overcomes the surface tension at the air–liquid interface around the nozzle, a fraction volume of the liquid is ejected out. The liquid stream is gradually expanded following the departure of the nozzle, without a physical restriction of the sidewall (t = 0.4 ms). As the liquid volume moves further away from the nozzle, a bottleneck forms (t = 0.8 ms) till its breakage (t = 1.2 ms) due to this flow instability.[53] This separated liquid continuously evolves into a spherical droplet under the influence of surface tension (t = 1.6 ms), while the residue fluid retracts back into the nozzle (t = 2.0 ms). Detailed image analysis of the droplet size (*i.e.*, droplet diameter) has been conducted on 3 different nozzles (of 95 μm, 126 μm and 270 μm diameter), respectively, and summarized in Fig. 4b–d. As expected, the diameters of the ejected droplets follow a Gaussian distribution, the random errors (denoted by the coefficient of variation, CV = 100 (S.D./Mean)) are measured in the range of 0.5–0.8%, and as a reference, the high-end commercial droplet generator (Microfab device) has a random error between 2.6–3.5%.[38]

According to the statistic theory, the random error of the targeted volume from accumulated dispensing can be expressed as:

$$\mathrm{CV}_{\mathrm{dispensed}} = \frac{3}{\sqrt{n}}\mathrm{CV}_{\mathrm{diameter}} = \frac{3}{\sqrt{n}}\frac{\sigma}{D} \quad (1)$$

where n stands for the number of dispensing, and D and σ are the mean diameter of the droplets and its standard

Published on 10 July 2018. Downloaded by University of Science and Technology of China on 4/15/2019 4:57:58 AM.

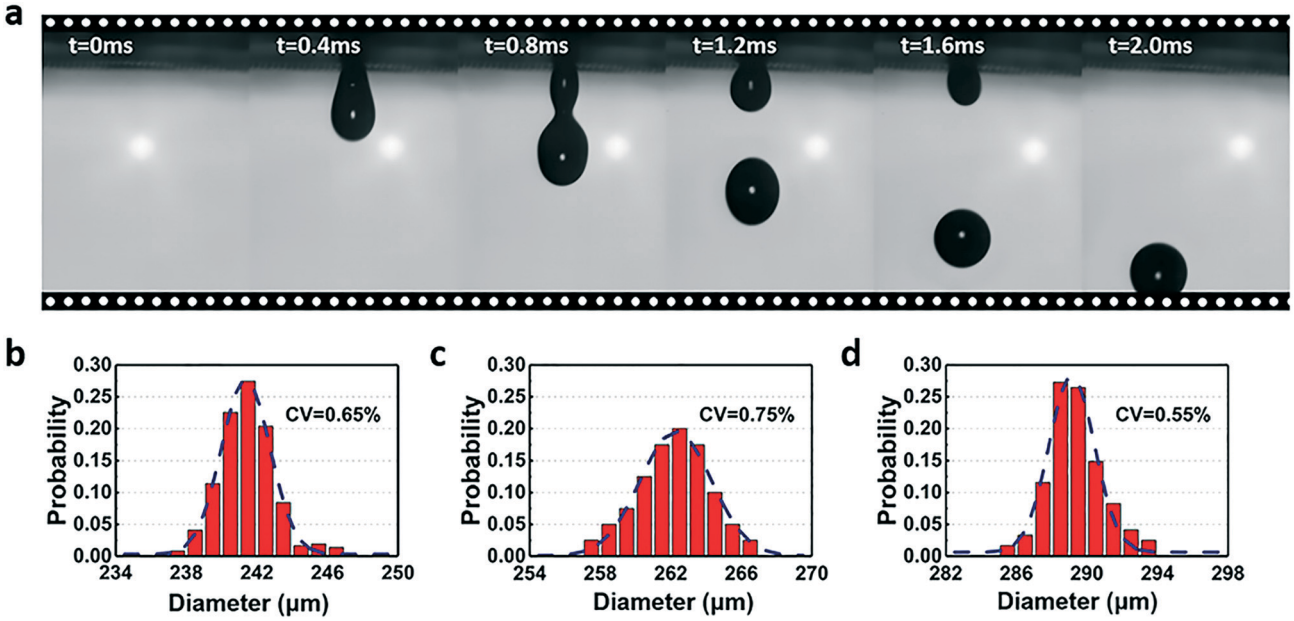

Fig. 4 a) Stroboscopic images showing droplet formation. Probability distribution histograms of droplet diameters for the three types of microfluidic pipetting chips with nozzle widths of b) 95 μm, c) 126 μm and d) 270 μm.

deviation, respectively (the detailed derivation is included in eqn S1 and S2 in the ESI†). As predicted by eqn (1), if the random error of a single droplet (of 6.54 nL) is measured around 2.3%, the overall random error for the accumulation of droplets of 0.1 μL liquid (*i.e.*, 15 droplet ejections) is 0.6%, as compared to that of the standard micropipette operations at nearly 50% (Table 1). These results imply that the laser-machined microfluidic pipetting device using the microfluidic impact printing principle can achieve significantly better accuracy and consistency in the transferred volume than a conventional pipetting device.

Alternatively, gravimetric characterization was used to calibrate the droplet volume by measuring its absolute mass. The numbers of printed droplets were from 100 to 500 at an interval of 100, considering the resolution of the microbalance. Each measurement of these ejected droplets was repeated four times and plotted in Fig. 5. The linear regression coefficients (R^2) were reported with high consistency greater than 0.999, demonstrating that the dispensing volume has a highly linear relationship with the ejection time. Moreover, the volume of a single droplet can be calculated from the total mass, which is 5.6 nL, 6.5 nL and 10.3 nL, respectively, from the different nozzle sizes (of 95 μm, 126 μm and 270 μm diameter), as shown in the legend of Fig. 5. The nozzle dimensions can be further tuned in terms of both its length and diameter by laser micromachining, from which a wider range of single droplet volumes can be hypothetically achieved in future. Furthermore, an experiment to evaluate the performance of dispensing protein solutions has been carried out and included in the ESI† (in Fig. S2†); the small coefficient of variation (CV = 2.4%) demonstrates that digital droplet pipetting can dispense many types of solutions with high precision.

Table 1 The total random errors of dispensed volume in the range of 0.1 μL to 0.5 μL by using the digital droplet pipette and an Eppendorf micropipette[54]

Volume (μL)	Number of droplets	Total random error (CV)	
		Digital droplet pipette	Standard micropipette
0.00654	1	±2.3%	—
0.1	15	±0.6%	±49.5%
0.25	38	±0.4%	±13.4%
0.5	76	±0.3%	±9.4%

Performance of direct dilution

To generate a conventional concentration profile, the serial dilution method is widely used in biological quantification

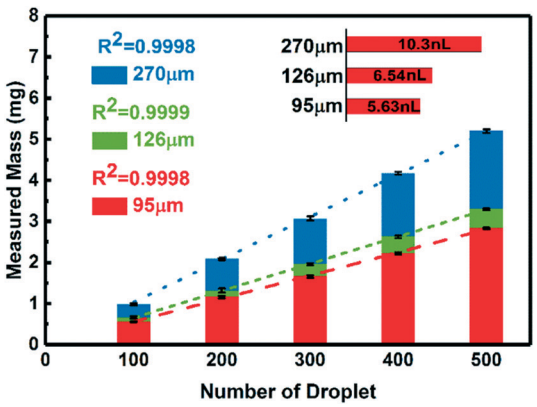

Fig. 5 Gravimetric method for characterizing the linearity of accumulated droplets from 100 to 500. The insert graph shows the different volumes of single-droplets related to different nozzle sizes.

This journal is © The Royal Society of Chemistry 2018

Published on 10 July 2018. Downloaded by University of Science and Technology of China on 4/15/2019 4:57:58 AM.

processes, such as IC_{50} analyses.[55,56] In such a scenario, an array of sample concentrations could be established by repeating dilution iterations at a pre-determined ratio, prepared using a standard pipette device.[45,57] Benefiting from the highly precise and automated digital droplet pipette, we proposed a direct dilution procedure, in which the targeted concentrations have been achieved by directly adding sample and buffer solutions together with designed volumes. The outcomes of direct dilution have been evaluated by the two distinct pipetting methods.

First of all, fluorescence characterization has been used to evaluate the random errors of diluted sodium fluorescein concentrations. The fluorescence intensities of the concentration gradients generated using the two kinds of pipetting methods are shown in Fig. 6a, with linear fitting curves drawn in dotted and dashed lines. The results from using the digital droplet pipetting method have been observed with a higher linear regression coefficient (R^2 = 0.9974) than that of using a standard micropipette (R^2 = 0.9899), demonstrating that the former method has a better precision and reliability in the dilution profile. Furthermore, the random errors of the experiments are analyzed and evaluated directly in Fig. 6b, compared with the theoretical analyses shown in dotted lines. The random errors of measured concentrations using digital droplet pipetting are within 3.8% in the range of 1 μg mL^{-1} to 10 μg mL^{-1} (given that the CV of single droplets is 2.3%), while those using a micropipette are up to 49% at the concentration of 1 μg mL^{-1}. The large errors caused by the micropipette are likely attributed to the imprecision of its principle, and markedly, it could consecutively accumulate and have an adverse impact on the results with further dilution iterations.[45] According to the calculations, the random errors using the two methods are within 1.8% and 41% at the same concentration, respectively (the detailed calculations of random errors are listed in Table S1 in the ESI†). Due to the omitted errors in the theoretical consideration (*i.e.* environment, microscope, human error), the calculated values are smaller in a margin of low concentration, however, they follow similar trends to the experimental findings. In conclusion, compared with a conventional micropipette, the digital droplet pipette can be extended to generate high-precision concentration gradients with predicable errors in a single-step dilution strategy.

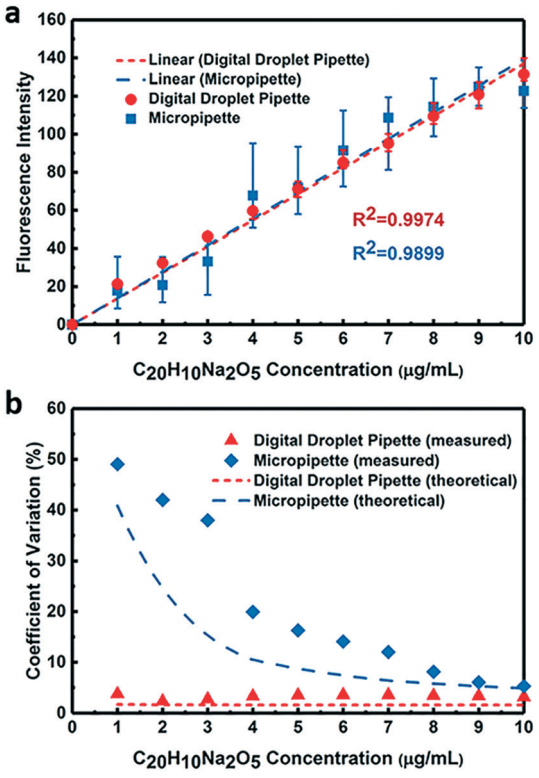

Fig. 6 Evaluation of the performance of the concentration dilution. a) Fluorescence intensities and b) the random errors of the concentration gradients generated using the digital droplet pipette and a micropipette.

Drug resistance assay

Drug therapies, including conventional chemotherapies, targeted molecular and nanodrug therapies, and recently developed immunotherapies, serve as the primary means of cancer treatment.[58] Specifically, doxorubicin, as a cytostatic drug, can intercalate into DNA double helices, inhibit topoisomerase II and cross-link DNA strands to disturb DNA function and induce DNA damage. Meanwhile doxorubicin is used in treatment of a wide variety of cancers as a chemotherapeutic agent as it can induce cell cycle arrest in cancer cells, thereby hampering killing of tumor cells.[59] To investigate the mechanisms of pharmaceutical actions of anticancer drugs, a number of analytical experiments have been conducted using the standard micropipetting platform.[59] Unfortunately, a significant amount of operational errors can be introduced by this existing approach as aforementioned, which could invalidate the findings and conclusions from the analysis. Herein, we have established a demonstration experiment for analyzing the effects of doxorubicin on cytotoxicity in A549 adenocarcinomic human alveolar basal epithelial cells at different concentrations using the direct dilution method presented in the previous section, which exhibits the high precision and high efficiency of the newly proposed droplet pipetting approach.

The experimental results are summarized in Fig. 7, where the scattered points show the cell viability data at different concentrations from 0.1 to 10 μM. Control experiments have been also carried out at concentrations from 0.5 μM to 10 μM, generated by using a micropipette. By examining the random errors, the droplet pipetting approach leads to minor and consistent random errors which are less than 6% in the range of 0.5 μM to 10 μM, whereas the errors created by the micropipette approach increase from 7.5% to 16.6% with reduced concentrations. Similar biological results have been reported by the Chovolou group,[59] who has carried out an apoptosis assay on different hct-116 human colon carcinoma cells using a micropipette method, illustrating consistent findings with our control experiment where large random

Published on 10 July 2018. Downloaded by University of Science and Technology of China on 4/15/2019 4:57:58 AM.

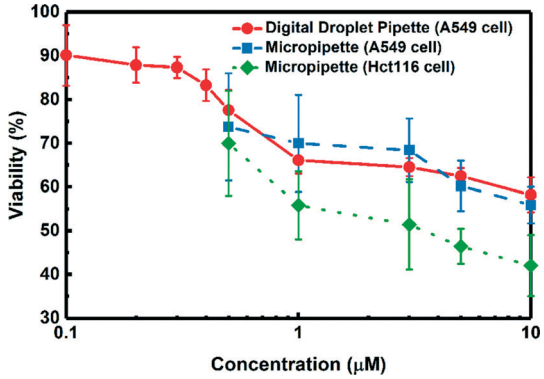

Fig. 7 Comparison of random errors of cell viability in a doxorubicin-induced apoptosis assay. The green scatter plot is from Chovolou group's work, which represents the effects of doxorubicin on different hct-116 human colon carcinoma cells using a micropipette.[59]

errors are found. Furthermore, benefiting from low-volume high-accuracy droplet pipetting, cell viability analysis beyond the conventional concentration limit (<0.5 μM) has been enabled by the direct dilution approach, from which the random errors of cell viability remain low (<7.7%) in the range between 0.1 and 0.5 μM. In brief, applying the direct dilution approach enabled by digital droplet pipetting to the drug resistance assay, it is confirmed that it has consistently lower random errors than the conventional micropipette, particularly at low concentrations.

Conclusions

In this paper, a new high-precision droplet pipetting method is introduced, in which a reversibly pluggable microfluidic pipetting chip with a superhydrophobically-modified surface and an in-plane nozzle can produce highly consistent nanoliter droplets. This digital droplet pipette has been configured onto a conventional pipette device with high resolution, high portability and easy programmability. In addition, the laser-induced nozzle superhydrophobicity minimizes the liquid adherence during both aspiration and dispensing, which further improves the precision of liquid handling and eliminates cross contamination. We have verified the high accuracy of the new pipetting method by two distinct characterization means. In particular, the precision of the dispensing volume has been improved from 49.5% to 0.6% at a transfer volume of 0.1 μL, as compared to that of conventional micropipetting. In comparison with conventional micropipetting, the concentration dilution enabled by digital droplet pipetting has also reduced the random errors from 49% to 3.8% at 1 μg mL^{-1}. Biological demonstration on analysis of anticancer pharmaceutical resistance has been conducted using the droplet pipetting approach, from which high-precision results have been achieved, compared with the conventional approach, particularly at low concentrations. In summary, with its advantages of nanoliter precision, user-friendly interface, low cost and non-contact dispensing, the novel microfluidic droplet pipetting system has the potential to contribute to a large array of biochemical and medical applications, in which high accuracy and low-processing volumes are both required.

Conflicts of interest

There are no conflicts to declare.

Acknowledgements

This research work was supported in part by the National Natural Science Foundation of China (No. 51675505) and the Joint Research Fund for Overseas Chinese, Hong Kong and Macao Young Scientists of the National Natural Science Foundation of China (Grant No. 51628502). Prof. Pan would like to acknowledge the support of the Superfund Research Program at UC Davis from the National Institutes of Health (No. 2P42ES004699), the Program for Guangdong Introducing Innovative and Entrepreneurial Teams (2016ZT06D631), and the Shenzhen Fundamental Research Program (JCYJ 20170413164102261). The authors would like to acknowledge Drs. Jinzhen Fan and Yongfan Men for their assistance in the experimental design, Han Li for his assistance in stroboscopic measurement and JunJun Tan for his assistance in gravimetric measurement.

Notes and references

1 F. Kong, L. Yuan, Y. F. Zheng and W. Chen, *J. Lab. Autom.*, 2012, **17**, 169–185.
2 Y. Liu, C. Liguo, L. Sun and W. Rong, *Proceedings of IEEE International Conference on Robotics and Automation*, Kobe, 2009.
3 G. Liu, C. Lanham, J. R. Buchan and M. E. Kaplan, *PLoS One*, 2017, **12**, e0174128.
4 R. E. Oosterbroek and A. V. D. Berg, *Lab-on-a-Chip: Miniaturized Systems for (BIO) Chemical Analysis and Synthesis*, Elsevier, Amsterdam, 1st edn, 2003.
5 A. J. Tudos, G. J. Besselink and R. B. Schasfoort, *Lab Chip*, 2001, **1**, 83–95.
6 P. S. Dittrich and A. Manz, *Nat. Rev. Drug Discovery*, 2006, **5**, 210–218.
7 P. L. Mills, D. J. Quiram and J. F. Ryley, *Chem. Eng. Sci.*, 2007, **62**, 6992–7010.
8 D. Janasek, J. Franzke and A. Manz, *Nature*, 2006, **442**, 374–380.
9 T. Vilkner, D. Janasek and A. Manz, *Anal. Chem.*, 2004, **76**, 3373–3386.
10 L. J. Kricka, *Clin. Chem.*, 1998, **44**, 6.
11 B. Larson, T. Moeller, P. Banks and J. J. Cali, *J. Biomol. Screening*, 2011, **16**, 895–902.
12 B. Larson, P. Banks, H. Sherman and M. Rothenberg, *J. Lab. Autom.*, 2012, **17**, 222–232.
13 B. Larson, P. Banks, H. Zegzouti and S. A. Goueli, *Assay Drug Dev. Technol.*, 2009, **7**, 573–584.
14 E. Whitehead, F. Rudolf, H. M. Kaltenbach and J. Stelling, *ACS Synth. Biol.*, 2018, **7**, 922–932.

 This journal is © The Royal Society of Chemistry 2018

Published on 10 July 2018. Downloaded by University of Science and Technology of China on 4/15/2019 4:57:58 AM.

15 Y. Zhu, Y. X. Zhang, W. W. Liu, Y. Ma, Q. Fang and B. Yao, *Sci. Rep.*, 2015, **5**, 9551.
16 S. Hin, N. Paust, M. Keller, M. Rombach, O. Strohmeier, R. Zengerle and K. Mitsakakis, *Lab Chip*, 2018, **18**, 362–370.
17 M. Keller, G. Czilwik, J. Schott, I. Schwarz, K. Dormanns, F. von Stetten, R. Zengerle and N. Paust, *Lab Chip*, 2017, **17**, 864–875.
18 D. J. Wilson and C. R. Mace, *Anal. Chem.*, 2017, **89**, 8656–8661.
19 F. Rainer and L. K. Heinz, *Accredit. Qual. Assur.*, 2016, **21**, 69–82.
20 J. Beroz and A. J. Hart, *Rev. Sci. Instrum.*, 2016, **87**, 115112.
21 E. Batista, L. Pinto, E. Filipe and A. M. H. van der Veen, *Measurement*, 2007, **40**, 338–342.
22 M. Berg, K. Undisz, R. Thiericke, P. Zimmermann, T. Moore and C. Posten, *J. Biomol. Screening*, 2001, **6**, 47–56.
23 C. W. Extrand and Y. Kumagai, *J. Colloid Interface Sci.*, 1996, **184**, 191–200.
24 D. Choi, H. Lee, D. J. Im, I. S. Kang, G. Lim, D. S. Kim and K. H. Kang, *Sci. Rep.*, 2013, **3**, 2037.
25 L. Kyle, F. Daniel, H. Ye and M. C. Dane, *J. Med. Lab. Diagn.*, 2015, **6**, 36–40.
26 G. W. Procop, L. M. Yerian, R. Wyllie, A. M. Harrison and K. Kottke-Marchant, *Am. J. Clin. Pathol.*, 2014, **141**, 718–723.
27 E. F. Gabriel, R. A. Dos Santos, E. O. Lobo-Junior, K. C. Rezende and W. K. Coltro, *Talanta*, 2017, **162**, 19–23.
28 E. Berthier, J. Warrick, B. Casavant and D. J. Beebe, *Lab Chip*, 2011, **11**, 2060–2065.
29 F. Dutka, A. S. Opalski and P. Garstecki, *Lab Chip*, 2016, **16**, 2044–2049.
30 K. Zhang, X. Han, Y. Li, S. Y. Li, Y. Zu, Z. Wang and L. Qin, *J. Am. Chem. Soc.*, 2014, **136**, 10858–10861.
31 K. Zhang, M. Gao, Z. Chong, Y. Li, X. Han, R. Chen and L. Qin, *Lab Chip*, 2016, **16**, 4742–4748.
32 H. N. Joensson and H. Andersson Svahn, *Angew. Chem., Int. Ed.*, 2012, **51**, 12176–12192.
33 H. Song, D. L. Chen and R. F. Ismagilov, *Angew. Chem., Int. Ed.*, 2006, **45**, 7336–7356.
34 A. B. Theberge, F. Courtois, Y. Schaerli, M. Fischlechner, C. Abell, F. Hollfelder and W. T. Huck, *Angew. Chem., Int. Ed.*, 2010, **49**, 5846–5868.
35 Y. Ding, E. Huang, K. S. Lam and T. Pan, *Lab Chip*, 2013, **13**, 1902–1910.
36 B. Li, J. Fan, J. Li, J. Chu and T. Pan, *Biomicrofluidics*, 2015, **9**, 054101.
37 J. Fan, F. Villarreal, B. Weyers, Y. Ding, K. H. Tseng, J. Li, B. Li, C. Tan and T. Pan, *Lab Chip*, 2017, **17**, 2198–2207.
38 A. Bsoul, S. Pan, E. Cretu, B. Stoeber and K. Walus, *Lab Chip*, 2016, **14**, 3351–3361.
39 R. E. Saunders and B. Derby, *Int. Mater. Rev.*, 2014, **59**, 430–448.
40 Y. Sun, X. Zhou and Y. Yu, *Lab Chip*, 2014, **14**, 3603–3610.
41 R. H. Colea, S.-Y. Tang, C. A. Siltanen, P. Shahia, J. Q. Zhang, S. Poust, Z. J. Gartnera and A. R. Abate, *Proc. Natl. Acad. Sci. U. S. A.*, 2017, **114**, 8728–8733.
42 I. H. Choi, H. Kim, S. Lee, S. Baek and J. Kim, *Biomicrofluidics*, 2015, **9**, 064102.
43 N. Hey, M. Freygang, H. Gruhler, H. Sandmaier and R. Zengerle, *Proceedings MEMS 98, IEEE, Eleventh Annual International Workshop on Micro Electro Mechanical Systems*, Heidelberg, 1998.
44 O. Gutmann, R. Niekrawietz, R. Kuehlewein, C. P. Steinert, B. d. Heij, R. Zengerle and M. Daub, *Sens. Actuators, A*, 2004, **116**, 187–194.
45 A. Ben-David and C. E. Davidson, *J. Microbiol. Methods*, 2014, **107**, 214–221.
46 M. Ma, R. M. Hill and G. C. Rutledge, *J. Adhes. Sci. Technol.*, 2008, **22**, 1799–1817.
47 K. Liu, Y. Tian and L. Jiang, *Prog. Mater. Sci.*, 2013, **58**, 503–564.
48 X. Wang, H. Hu, Q. Ye, T. Gao, F. Zhou and Q. Xue, *J. Mater. Chem.*, 2012, **22**, 7.
49 G. Li, J. Li, C. Zhang, Y. Hu, X. Li, J. Chu, W. Huang and D. Wu, *ACS Appl. Mater. Interfaces*, 2015, **7**, 383–390.
50 D. Wu, J.-N. Wang, S.-Z. Wu, Q.-D. Chen, S. Zhao, H. Zhang, H.-B. Sun and L. Jiang, *Adv. Funct. Mater.*, 2011, **21**, 2927–2932.
51 J. Yong, Q. Yang, F. Chen, D. Zhang, U. Farooq, G. Du and X. Hou, *J. Mater. Chem. A*, 2014, **2**, 5499–5507.
52 Y. Lu, L. Yu, Z. Zhang, S. Wu, G. Li, P. Wu, Y. Hu, J. Li, J. Chu and D. Wu, *RSC Adv.*, 2017, **7**, 11170–11179.
53 B. Derby, *Annu. Rev. Mater. Res.*, 2010, **40**, 395–414.
54 *Eppendorf Research® plus – Technical Datas*, https://online-shop.eppendorf.us/eshopdownload/downloadbykey/62903_186.
55 K. R. Aneja, *Experiments in Microbiology, Plant Pathology and Biotechnology*, New Age International, New Delhi, 4th edn, 2003.
56 F. Rainey and A. Oren, *Extremophiles: Methods in Microbiology*, Elsevier, Amsterdam, 1st edn, 2006.
57 A. J. Hedges, *Int. J. Food Microbiol.*, 2002, **76**, 207–214.
58 B. A. Chabner and T. G. Roberts Jr, *Nat. Rev. Cancer*, 2005, **5**, 65–72.
59 R. Lupertz, W. Watjen, R. Kahl and Y. Chovolou, *Toxicology*, 2010, **271**, 115–121.